Neuronal induction of BNIP3-mediated mitophagy slows systemic aging in *Drosophila*

Edward Schmid
University of California, Los Angeles
Jung-Hoon Pyo
University of California, Los Angeles
David Walker (davidwalker@ucla.edu)
University of California, Los Angeles

Article

Keywords: Autophagy, Mitophagy, Neuronal aging, Intestinal barrier dysfunction, Intestinal stem cell, Mito-QC.

Posted Date: April 27th, 2021

DOI: https://doi.org/10.21203/rs.3.rs-438556/v1

Version of Record: A version of this preprint was published at Nature Aging on May 16th, 2022. See the published version at https://doi.org/10.1038/s43587-022-00214-y.

Abstract

The effects of aging on the brain are widespread and present at both the cellular and functional level. Mitochondrial dysfunction is a hallmark of brain aging, but, the interplay between mitochondrial quality control, neuronal aging, and organismal health is not well understood. Here, we show that aging leads to a decline in mitochondrial autophagy (mitophagy) in the *Drosophila* brain and a concomitant increase in mitochondrial content. We find that induction of BCL2-interacting protein 3 (BNIP3), a mitochondrial outer membrane protein, in the adult nervous system induces mitophagy and prevents the accumulation of dysfunctional mitochondria in the aged brain. Importantly, neuronal induction of BNIP3-mediated mitophagy increases organismal longevity and healthspan. Furthermore, neuronal BNIP3-mediated mitophagy improves mitochondrial homeostasis and proteostasis in aged muscle, indicating cell non-autonomous effects. In addition, neuronal BNIP3-mediated mitophagy improves intestinal homeostasis in aged flies. Our findings identify BNIP3 as a novel therapeutic target to counteract brain aging and prolong overall organismal health with age.

Introduction

Brain function declines with age, manifesting as impairments in learning and memory, attention, decision-making speed, sensory perception, cognitive function and motor coordination (Alexander et al., 2012; Dykiert et al., 2012; Levin et al., 2014). In addition, aging is the major risk factor for the development of neurodegenerative diseases, including Alzheimer's disease and Parkinson's disease. As the burden of age-related neurodegenerative disorders increases at an exponential rate all over the world (Prince et al., 2015), there is a considerable need for a better understanding of the mechanisms of brain aging and relationship to organismal health and longevity. Examination of the molecular and cellular changes that occur during brain aging indicate significant overlap with the hallmarks of aging in other organ systems (Lopez-Otin et al., 2013; Mattson and Arumugam, 2018). Indeed, one of the most extensively studied hallmarks of brain aging is the accumulation of dysfunctional mitochondria, which has also been implicated in organismal aging and neurodegenerative diseases (Grimm and Eckert, 2017; Mattson and Arumugam, 2018; Sun et al., 2016). Neurons are particularly vulnerable to mitochondrial dysfunction given that they are post-mitotic differentiated cells relying almost exclusively on the oxidative phosphorylation system to sustain their high energy needs. Hence, identifying interventions that could prevent the accumulation of dysfunctional mitochondria in the aging brain could provide novel approaches to counteract age-related health decline.

Autophagy, a lysosomal degradation pathway that plays essential roles in development, tissue homeostasis and disease pathogenesis (Levine and Kroemer, 2008), has emerged as an important modulator of tissue and organismal aging (Hansen et al., 2018). In this process, cellular materials (referred to as autophagic cargo) are sequestered by double-membrane vesicles known as autophagosomes, and delivered to the lysosome for degradation (Feng et al., 2014). Mitochondrial autophagy (mitophagy) is a type of cargo-specific autophagy that mediates the removal of dysfunctional mitochondria (Pickles et al., 2018; Youle and Narendra, 2011). Studies in diverse species, including

humans, have reported an age-related decline in mitophagy (Drummond et al., 2014; Rana et al., 2017; Sun et al., 2015). Moreover, studies in invertebrate models have shown that interventions that facilitate mitophagy can prolong lifespan and improve tissue homeostasis during aging (Aparicio et al., 2019; D'Amico et al., 2019; Rana et al., 2017; Rana et al., 2013; Ryu et al., 2016). Hence, there is an emerging understanding that mitophagy represents a key pathway to preserve mitochondrial function, and, hence, cell and tissue health, during aging (Hansen et al., 2018; Martinez-Vicente, 2017; Palikaras et al., 2015, 2016; Sun et al., 2016).

The molecular mechanisms of mitophagy involve coordinating autophagy induction with mitochondrial priming for autophagic recognition (Onishi et al., 2021; Pickrell and Youle, 2015). BNIP3 is a Bcl-2 family protein with an atypical BH3 domain that primarily localizes at the mitochondrial outer membrane. It has become apparent that BNIP3 can exert multiple cellular effects involving direct or indirect interactions with mitochondria (Dorn, 2010). Initial studies reported that BNIP3 can act as a pro-apoptotic protein, inducing cell death and mitochondrial dysfunction (Burton and Gibson, 2009; Kale et al., 2018; Kubli et al., 2007; Regula et al., 2002). However, it has also been shown that BNIP3 can act as a potent inducer of autophagy/mitophagy without inducing cell death in multiple cell types (Bellot et al., 2009; Dorn, 2010; Rikka et al., 2011; Zhang et al., 2016). More specifically, BNIP3 has been shown to serve as an autophagy receptor for the binding of mitochondria to ATG8/LC3 on the autophagosome via its N-terminal LC3-interacting region (Hanna et al., 2012; Onishi et al., 2021; Zhu et al., 2013). It has also been shown that BNIP3 interacts with PINK1 to suppress its cleavage, leading to enhanced mitochondrial clearance via mitophagy (Zhang et al., 2016). BNIP3-mediated mitophagy has been reported to exert pro-survival effects in certain pathological conditions (Glick et al., 2012; Li et al., 2018; O'Sullivan et al., 2015; Tang et al., 2019; Zhang et al., 2016). However, the impact of BNIP3 induction during aging on mitochondrial homeostasis and organismal health are not known.

The role of BNIP3 in mitophagy induction prompted us to determine whether BNIP3 could modulate neuronal and/or organismal aging. First, we examined whether BNIP3 can improve mitochondrial homeostasis in the aging *Drosophila* brain. We show that in control flies there is a striking accumulation of dysfunctional mitochondria in aged brains. Up-regulation of BNIP3 in the adult nervous system is sufficient to induce mitophagy and prevent the accumulation of dysfunctional mitochondria in an autophagy-dependent manner. In assessing organismal aging, neuronal BNIP3-mediated mitophagy is sufficient to prolong lifespan and improve several markers of healthspan in aged flies. Interestingly, we find that neuronal BNIP3 induction improves markers of both mitochondrial homeostasis and proteostasis in aged muscle in an autophagy-dependent manner. In addition, neuronal BNIP3 induction delays intestinal stem cell aging and maintains intestinal barrier function also in an autophagy-dependent manner. Together, these findings indicate that functional up-regulation of BNIP3 in the aging brain may represent a novel therapeutic strategy to promote healthy aging in elderly humans.

Results

Neuronal induction of BNIP3 counteracts the accumulation of dysfunctional mitochondria in the aged brain

Having complex systems biology with many parallels to human physiology, the fruit fly *Drosophila* is an excellent model to study the role of mitochondria homeostasis in aging and lifespan determination (Cho et al., 2011). Here, we set out to examine the interplay between BNIP3 induction and mitochondrial homeostasis in the aging fly brain. Accordingly, we used Gene-Switch driver lines to express a *UAS-hBNIP3-HA* (hereafter *BNIP3*) transgene created by (Zhang et al., 2016). The Gene-Switch system enables all flies in a given experiment to share genetic background and developmental conditions, only differing in whether they are given the inducing agent (RU486) or vehicle (ethanol) in the food during adulthood (Osterwalder et al., 2001). To investigate the effects of *BNIP3* induction in neurons, we used the pan-neuronal *Elav-Gene-Switch* (*elav*GS) driver line to induce *BNIP3* expression specifically in neurons during adulthood (Poirier et al., 2008). We first validated RU486-dependent transgene expression in *elavGS>UAS-BNIP3* flies using immunofluorescence (IF) microscopy by staining for the HA tag in fly brains (Extended Data Fig. 1a,b). No HA staining was detected in peripheral tissues, including the gut and indirect flight muscles (data not shown). Previous studies in *Drosophila* have reported age-related alterations in mitochondrial morphology and function in muscle tissue and in mitochondria isolated from whole animals (Aparicio et al., 2019; Brandt et al., 2017; Ferguson et al., 2005; Rana et al., 2017; Rana et al., 2013; Walker and Benzer, 2004). However, little is known about alterations in mitochondrial homeostasis in the aging fly brain. Therefore, we used IF microscopy to investigate mitochondrial morphology and content in aging *Drosophila* brains. Compared to brains from young adult flies, aged brains showed a striking accumulation of mitochondrial content (Fig. 1a,b). The human brain shrinks during normal aging, with reductions in both gray and white matter and an associated enlargement of the cerebral ventricles (Mattson and Arumugam, 2018). We noted a similar neuronal loss in aged *Drosophila* brains by nuclei staining (Extended Data Fig. 2a,b). Neuronal-specific induction of *BNIP3* significantly reduced brain mitochondrial content to levels similar to those detected in young animals (Fig. 1a,b), supporting a role for BNIP3 in mitochondrial homeostasis. Remarkably, neuron-specific up-regulation of BNIP3 also counteracted neuronal loss detected in age-matched controls (Extended Data Fig. 2a,b).

To provide an additional marker of mitochondrial content, we examined mitochondrial (mt)DNA levels in the brains of young and aged flies. Consistent with an age-related accumulation of mitochondria, we observed an increase in mtDNA in aged brains that was prevented with neuronal-specific induction of BNIP3 (Fig. 1c,d). We confirmed these changes to mtDNA levels in fly heads using quantitative polymerase chain reaction (qPCR) (Fig. 1e). To assess mitochondrial function in aging brains, we examined mitochondrial membrane potential using the potentiometric dye tetramethylrhodamine, ethyl ester (TMRE). While brain mitochondria showed reduced TMRE intensity with age, neuronal induction of *BNIP3* resulted in significantly higher mitochondrial membrane potential compared to age-matched controls (Fig. 1f,g). Importantly, RU486 treatment and expression of a control transgene in *elavGS>UAS-GFP* flies had no effect on mitochondria accumulation in aging brains (Extended Data Fig. 3a,b). Collectively, these data demonstrate that there is an accumulation of dysfunctional mitochondria in the aged fly brain that can be counteracted by neuronal BNIP3 induction.

Neuronal BNIP3 induction promotes mitophagy in the aged brain

BNIP3 has been proposed to function as a mitophagy receptor (Onishi et al., 2021). However, the relationships between BNIP3, mitophagy and mitochondrial function during neuronal aging are not known. Endogenous LC3/ATG8 levels are commonly used as steady-state autophagy markers to allow visualization of autophagosomes (Klionsky et al., 2021). Studies in both worms (Chang et al., 2017) and flies (Aparicio et al., 2019) have reported an age-related increase in autophagosomes, reflective of a decline in autophagic activity. To explore the interplay between BNIP3 induction and autophagy, we examined the levels of endogenous ATG8a in aging brains using IF microscopy. Consistent with findings in the neurons of aged *C. elegans* (Chang et al., 2017), we observed a striking increase in ATG8a levels in aged fly brains that was abrogated with neuronal BNIP3 induction (Extended Data Fig. 4a,b), consistent with improved autophagic activity. To further evaluate changes to brain autophagy with age and with BNIP3 induction, we used a reporter line expressing GFP-mCherry-ATG8a ubiquitously under the control of the ATG8a promoter (Lee et al., 2016). Due to the pH-sensitive properties of GFP, ATG8a in acidic environments—autolysosomes—will display mCherry-only foci. When overexpressing BNIP3 in neurons, we detected significantly more red-only puncta, indicating an increase in autolysosomes (Fig. 2a,b). Next, to evaluate changes more specifically to mitophagy, we used the recently characterized mitophagy reporter line, mito-QC, that encodes a tandem GFP-mCherry fusion protein that is targeted to the outer mitochondrial membrane (Lee et al., 2018). With this tool, mitochondria degraded in the acidic microenvironment of lysosomes (mitolysosomes) will appear as mCherry-only puncta (McWilliams et al., 2016). In agreement with its reported role as a mitophagy receptor, BNIP3 up-regulation in neurons of mito-QC flies resulted in significantly more mCherry-only foci (mitolysosomes) in aged brains compared to controls (Fig. 2c,d). Notably, neuronal induction of BNIP3 at midlife for both one or two weeks (days 30-37 or 30-44) was sufficient to increase mitolysosomes in aging brains (Extended Data Fig. 5a-d).

A key prediction of the mitophagy model is that the ability of BNIP3 to improve mitochondrial homeostasis will depend upon the autophagy pathway. *Atg1* (the homolog of mammalian ULK1) is a Ser/Thr protein kinase essential in the initiation of autophagosome formation (Nakatogawa et al., 2009). To test if the observed improvements to mitochondrial homeostasis associated with neuronal *BNIP3* upregulation (Fig. 1) are dependent on autophagy, we generated *elavGS>UAS-Atg1-RNAi,UAS-BNIP3* flies. Brains from flies with concomitant neuronal induction of *Atg1-RNAi* and *BNIP3* showed age-related accumulation of mitochondria similar to uninduced controls (Fig. 2e,f). In agreement with mitochondrial content, flies with neuronal induction of *Atg1-RNAi* and *BNIP3* showed impaired mitochondrial membrane potential in aged brains (Fig. 2g,h) in contrast to flies expressing *BNIP3* without *Atg1-RNAi* induction in neurons (Fig. 1f,g). BNIP3 expression was confirmed in brains of *elavGS>UAS-Atg1-RNAi,UAS-BNIP3* flies upon RU486 treatment (Extended Data Fig. 6a,b). These findings indicate an autophagy-dependent mechanism to *BNIP3*-induced changes to mitochondrial content and function in aging neurons.

Neuronal *BNIP3* upregulation improves organismal healthspan and extends lifespan

Having observed that neuronal induction of *BNIP3* improved mitochondrial homeostasis in aged brains, we decided to investigate potential impact on organismal health by examining a number of markers of healthspan. Remarkably, flies up-regulating *BNIP3* in neurons had significantly longer lifespans than controls (Fig. 3a, Extended Data Table 1). Interestingly, midlife neuronal upregulation of *BNIP3* was sufficient to extend maximum lifespan of flies (Extended Data Fig. 5e). To confirm that lifespan extension was a result of *BNIP3* induction and not an artifact of any transgene expression and/or RU486 exposure, *elavGS>UAS-GFP* flies were generated. RU486-mediated GFP expression in adult neurons failed to prolong lifespan compared to controls (Extended Data Fig. 7a). Since changes to food intake can influence lifespan, we tested if neuronal *BNIP3* induction affected feeding behavior. Using the Con-Ex feeding assay (Shell et al., 2018), we failed to observe alterations in food consumption and excretion upon neuronal *BNIP3* induction (Extended Data Fig. 8a). Likewise, neuronal expression of GFP had no observable effect on feeding behavior (Extended Data Fig. 7b). To understand if the lifespan benefits of neuronal *BNIP3* could be recapitulated when targeting BNIP3 induction in other cell types, *daughterless (da)GS*, *Act88FGS*, and *5966GS* drivers were used to express *BNIP3* ubiquitously, in muscles, and in intestinal enterocytes, respectively. However, none of these interventions increased fly lifespan (Extended Data Fig. 9a,b,c). Hence, we conclude that neuronal up-regulation of BNIP3 is key to the observed prolongevity phenotype.

To assess how aging health could be affected by neuronal *BNIP3* induction, we tested several behavioral readouts. Throughout the course of their lifespan, RU486-activated *elavGS>UAS-BNIP3* flies showed delayed reduction in locomotor activity associated with aging (Fig. 3b,c). Furthermore, these flies showed significant improvement in climbing endurance assays (Fig. 3d). No change was detected in climbing ability during aging in control flies expressing GFP in neurons (Extended Data Fig. 7c). Neuronal *BNIP3* upregulation also conferred an increase in spontaneous daytime activity with no detectable nighttime restlessness in aged flies (Fig. 3e,f). Some lifespan extension strategies, including dietary restriction, are associated with reduced reproductive fitness (Partridge et al., 2005). However, we failed to detect a change in fertility in flies with neuronal *BNIP3* induction (Extended Data Fig. 8b). Overall, these data reveal that upregulating *BNIP3* in neurons prolongs not only lifespan, but, also several markers of healthspan.

With changes to mitochondrial homeostasis in flies expressing *BNIP3* in neurons being dependent on *Atg1* (Fig. 2e-h), we decided to test if lifespan and healthspan improvements were also contingent on autophagy. Notably, concomitant induction of *BNIP3* and *Atg1-RNAi* in neurons prevented the lifespan extension associated with *BNIP3* induction alone (Fig. 3g). Likewise, RU486-activated *elavGS>UAS-Atg1-RNAi,UAS-BNIP3* flies showed no detectable improvement in climbing endurance assays (Fig. 3h) or in spontaneous activity (Fig. 3i,j) compared to control flies. Hence, the ability of neuronal BNIP3 to prolong healthspan and lifespan is also dependent on autophagy.

Neuronal induction of BNIP3 improves mitochondrial homeostasis and proteostasis in aged muscle

Aging is a systemic process associated with the physiological decline of multiple organ systems. There is an emerging understanding that modulating components of neuronal aging can impact systemic aging (Miller et al., 2020; Weir and Mair, 2016). Hence, we set out to explore whether facilitating mitophagy in aged neurons could impact hallmarks of muscle aging. *Drosophila* flight muscle is an energy-demanding tissue in which mitochondria are tightly organized in rows between actin filaments. Previous work has revealed a midlife shift toward a more elongated mitochondrial morphology, which is linked to impaired mitophagy and the accumulation of dysfunctional mitochondria in aged flight muscle (Aparicio et al., 2019; Rana et al., 2017). Accordingly, we used IF microscopy to investigate mitochondrial homeostasis in the flight muscles of *Drosophila* in which *BNIP3* is upregulated in neurons. Remarkably, neuronal induction of BNIP3 led to smaller mitochondria in aged flight muscles (Fig. 4a,b). Inducing GFP in neurons, as a control, had no effect on mitochondrial size in aged muscle (Extended Data Fig. 10a,b). Consistent with a decrease in mitochondrial content, neuronal induction of *BNIP3* reduced the amount of mtDNA in aged muscle (Fig. 4c,d). To understand how changes in mitochondrial morphology and content related to mitochondrial function in aged muscle, TMRE was used to assess mitochondrial membrane potential. Importantly, neuronal BNIP3 up-regulation significantly improved mitochondrial membrane potential in aged muscle (Fig. 4e,f).

Another major cellular hallmark of aging is the loss of protein homeostasis (proteostasis) (Lopez-Otin et al., 2013). *Drosophila* flight muscle accumulates aggregates of ubiquinated proteins during aging, consistent with a loss of proteostasis (Aparicio et al., 2019; Demontis and Perrimon, 2010; Rana et al., 2017; Rana et al., 2013; Schinaman et al., 2019; Ulgherait et al., 2014). Here, we set out to determine whether neuronal BNIP3-mediated mitophagy can impact muscle proteostasis during aging. In doing so, we observed that neuronal *BNIP3* induction significantly reduced age-associated muscle protein aggregates (Fig. 4g,h). Taken together, these data reveal non-cell autonomous changes to aging muscle in flies with neuronal *BNIP3* induction.

Neuronal induction of *BNIP3* improves intestinal homeostasis during aging

Intestinal homeostasis is critical to maintain organismal healthspan and longevity (Jasper, 2015; Rera et al., 2013). In *Drosophila,* intestinal aging is associated with altered intestinal stem cell (ISC) behavior, microbial dysbiosis, and loss of barrier function (Clark et al., 2015; Jasper, 2015; Li and Jasper, 2016; Rera et al., 2012). During aging, the number of mitotic cells in the *Drosophila* midgut increases due to ISC hyperproliferation and misdifferentiation (Biteau et al., 2008; Li and Jasper, 2016). This age-induced hyperplasia can be assayed by scoring phosphorylated histone H3 (pH3) in the aging intestine. To examine the impact of neuronal BNIP3 up-regulation on intestinal homeostasis, we examined the number of $pH3^+$ cells in young and aged intestines. Remarkably, we found that inducing *BNIP3* in neurons significantly reduced pH3 counts in the posterior midgut compared to control flies (Fig. 5a,b).

Little is known about changes to enterocyte mitochondrial dynamics as organisms age. Using IF microscopy, we found that mitochondrial content significantly increased in the enterocytes of the posterior midgut of aged flies compared to young controls (Fig. 5c,d). Interestingly, neuronal induction of

BNIP3 resulted in reduced mitochondrial content in aged intestinal enterocytes (Fig. 5c,d). Flies expressing control GFP in neurons showed no change to enterocyte mitochondrial content compared to age-matched guts (Extended Data Fig. 11a,b). In recent years, intestinal barrier dysfunction has emerged as a conserved feature of aged organisms that has been linked to systemic inflammation, organismal health decline and mortality (Clark et al., 2015; Dambroise et al., 2016; Hu and Jasper, 2017; Kavanagh et al., 2016; Rera et al., 2011; Rera et al., 2012; Thevaranjan et al., 2017). To determine whether neuronal BNIP3 induction can impact intestinal barrier function, we examined intestinal integrity during aging via the 'Smurf assay' (Rera et al., 2011; Rera et al., 2012). Remarkably, we observed a delay in the onset of intestinal barrier dysfunction upon neuronal expression of *BNIP3* (Fig. 5e). To determine whether improved intestinal barrier function was linked to changes in gut bacteria, we utilized qPCR with universal primers to the bacterial 16S rRNA gene to characterize alterations in microbiota dynamics in response to neuronal BNIP3 expression. Interestingly, we failed to see a significant change in gut bacterial load in aged flies with neuronal BNIP3 expression (Extended Data Fig. 12). Together, these data indicate that neuronal BNIP3 upregulation can significantly delay the onset of muscle aging and intestinal aging markers.

Neuronal *BNIP3* induction requires autophagy to slow muscle aging and intestinal aging

Neuronal up-regulation of *BNIP3* improved mitochondrial homeostasis in the brain in an autophagy-dependent manner. Here, we set out to determine whether the impact of neuronal BNIP3 induction on muscle aging and intestinal aging requires autophagy. Remarkably, flies expressing *Atg1-RNAi* and *BNIP3* in neurons showed significantly larger mitochondria in the indirect flight muscle compared to both young and age-matched control flies (Fig. 6a,b). Furthermore, mitochondria in the indirect flight muscles of flies neuronally expressing *Atg1-RNAi* and *BNIP3* showed significantly reduced membrane potential compared to young flies (Fig. 6c,d). Therefore, neuronal BNIP3 requires autophagy to counteract the accumulation of dysfunctional mitochondria in aged muscle. In a similar fashion, we examined whether the impact of neuronal BNIP3 on intestinal homeostasis during aging requires autophagy. In doing so, we found that pH3 counts in the posterior midgut were significantly higher in both aged control flies and in aged flies expressing *ATG1-RNAi* and *BNIP3* in neurons compared to young controls, indicating impaired gut homeostasis (Fig. 6e,f). In addition, we find that co-expression of *ATG1-RNAi* with *BNIP3* in adult neurons prevents the ability of BNIP3 to counteract the accumulation of mitochondria in aged intestinal cells (Fig. 6g,h). Finally, we also find that the ability of neuronal BNIP3 to delay the onset of intestinal barrier dysfunction during aging is autophagy-dependent. *elavGS>UAS-Atg1-RNAi,UAS-BNIP3* flies showed no difference in the number of 'Smurf' flies when given RU486 compared to vehicle-fed controls (Fig. 6i). Together, these data reveal that changes to cellular and physiological hallmarks of muscle and intestinal aging associated with *BNIP3* induction in neurons is dependent on the activity of neuronal autophagy.

Discussion

Mitochondria produce ATP and are, therefore, critical for neuronal health. Mitochondrial dysfunction is one of the most well-studied cellular hallmarks of brain aging and age-onset neurodegenerative diseases (Grimm and Eckert, 2017; Mattson and Arumugam, 2018; Sun et al., 2016). Decades of research in model organisms and clinical studies have revealed a decline in mitochondrial function in aged brain tissue. However, the underlying mechanisms that lead to a loss of mitochondrial activity with age are not yet understood. One potential explanation for an age-related decline in mitochondrial function would be a loss of mitochondrial content with age. However, at present, a clear understanding of how mitochondrial content changes during brain aging is missing. Using the fruit fly *Drosophila* as a model organism, we find that there is a striking increase in mitochondrial content in the aged brain. Consistent with previous studies, which have reported an age-related decline in mitochondrial respiratory function in whole flies (Brandt et al., 2017) and dissected muscle tissue (Ferguson et al., 2005), we find that mitochondria that accumulate in the aged brain show reduced mitochondrial membrane potential. Our findings were, in part, focused on a specific region of the fly brain (the optic lobe). It is beyond the scope of this study to document age-related changes in mitochondrial content and function in all brain regions. However, in future work, it would be interesting to examine whether there is regional or cell-type specificity in this regard. Defects in mitophagy, a mitochondrial quality control mechanism enabling the degradation of damaged and superfluous mitochondria, have been implicated in a number of pathological contexts, including age-onset neurodegeneration (Lou et al., 2020; Palikaras et al., 2018). Here, we have observed that brain aging is linked to a decline in mitophagy in *Drosophila*. These findings lead us to conclude that a decline in mitochondrial quality control, rather than a loss of mitochondrial content, is a major factor underlying age-onset mitochondrial dysfunction in the fly brain. A logical extension of this idea is that targeting mitophagy to improve mitochondrial homeostasis in the aging brain may prove a viable strategy to forestall brain aging phenotypes.

The major finding of this study is the identification of BNIP3 as a novel therapeutic target to counteract mitochondrial dysfunction in the aging brain and prolong healthy lifespan. BNIP3 has been reported to play roles in various cellular processes, including mitochondrial dysfunction, mitochondrial fragmentation, mitophagy and apoptosis (Burton and Gibson, 2009; Zhang and Ney, 2009). Hence, BNIP3 cannot be indiscriminately categorized as pro- or anti-apoptotic in function. Furthermore, BNIP3 is expressed in various tissues and is regulated by several different molecules under a variety of conditions (Gao et al., 2020). In the present study, we find that up-regulation of BNIP3 in adult neurons counteracts the accumulation of dysfunctional mitochondria in the aged brain. Interestingly, we observe that neuronal BNIP3 expression also counteracted age-related neuronal loss. Hence, it would appear unlikely that a pro-apoptotic mechanism underlies the observed effects on mitochondrial content. Most importantly, we find that the ability of BNIP3 to prevent the accumulation of mitochondria is dependent upon the autophagy pathway. Moreover, BNIP3 mediated improvements in organismal healthspan also require autophagy. The simplest interpretation of these findings is that BNIP3 induces mitophagy to improve mitochondrial homeostasis in the aged brain, delaying organismal health decline and mortality. Interestingly, we find that neuronal up-regulation of BNIP3 in middle-aged flies is sufficient to facilitate mitophagy and promote longevity. This could prove important when considering the development of

interventions based upon our findings. At the same time, however, we note that the prolongevity benefits of BNIP3 up-regulation may be specific to neuronal manipulations. Indeed, we failed to detect lifespan extension upon BNIP3 up-regulation using ubiquitous, muscle-specific, or intestine-specific manipulations. It is interesting to speculate that BNIP3 activation in non-neuronal cells may compromise tissue and organismal health via pro-apoptotic mechanisms.

It is intriguing that neuronal BNIP3 up-regulation produced alterations in cellular and physiological markers of aging in aged muscle and intestine. More specifically, neuronal BNIP3 was able to improve both mitochondrial homeostasis and proteostasis in aging muscle. In addition, neuronal BNIP3 was able to delay markers of intestinal stem cell aging and mitochondrial accumulation in the aged intestine. Finally, neuronal BNIP3 up-regulation delayed the onset of intestinal barrier dysfunction in aged flies. We interpret these findings to support a model in which healthy mitochondrial function in the aging brain is essential to maintain muscle and intestinal health. One potential future research direction would be to uncover the potential role of inter-organ signaling in mediating these effects.

Materials And Methods

Fly stocks

The fly strain *UAS-hBNIP3-HA* was kindly provided by Z. Zhang (Central South University, Changsha, Hunan, China). *Elav–GeneSwitc*h (*ElavGS*) was provided by H. Keshishian (Yale University, New Haven, CT, USA), *daughterless-GeneSwitch* (*daGS*) was provided by H. Tricoire (Universite´ Paris Diderot–Paris7, Paris, France), *5966-GeneSwitch* (*5966GS*) was provided by H. Jasper (Genentech, San Francisco, CA, USA) and *Actin88F-GeneSwitch* (Act88FGS) was provided by F. Demontis (St. Jude Children's Research Hospital, Memphis, TN, USA).GFP-mCherry-Atg8a was provided by Eric Baehrecke (University of Massachusetts Medical School, Worcester, MA, USA). *UAS-mito-QC* was provided by Alexander J. Whitworth (University of Cambridge, UK). UAS-Atg1-RNAi (16133) line was received by Vienna Drosophila RNAi Center (VDRC).

Fly Husbandry and Lifespan Analysis

Flies were reared in vials containing cornmeal medium (1% agar, 3% yeast, 1.9% sucrose, 3.8% dextrose, 9.1% cornmeal, 1.1% acid mix, and 1.5% methylparaben, all concentrations given in wt/vol). Flies were collected under light nitrogen-induced anesthesia and housed at a density of 30 female flies per vial. All flies were kept in a humidified, temperature-controlled incubator with 12h:12h dark:light cycle at 25 °C. RU486 was dissolved in ethanol and administered in the media while preparing food. Flies were flipped to fresh vial every 2–3 days and scored for death.

Immunostaining and Image analysis

For brain and muscle immunostaining, flies were fixed 3.7% formaldehyde in phosphate buffered saline (PBS) for 20 min. After fixation hemi-thoraces and brains were dissected and fixed again for 5 min. For

gut immunostaining, intact adult guts were dissected and fixed for 30 min in 4% formaldehyde in PBS for 30 min, dehydrated for 5 min in each 50%, 75%, 87.5%, and 100% methanol, and rehydrated for 5 min in each 50%, 25%, and 12.5% methanol in 0.2% Triton X-100 in PBS (PBST) as previously described. Samples were then rinsed 3 times for 10 min with PBST and blocked in 3% BSA in PBST (PBST-BSA) for 1 hour. Primary antibodies were diluted in PBST-BSA and incubated overnight at 4°C. Primary antibodies used were: mouse anti-ATP5a 1:250 (15H4C4, abcam); rabbit-anti-HA 1:250 (CellSignaling); mouse-anti-FK2 1:250 (BML-PW8810-0500, ENZO); rabbit-anti-atg8a 1:250 (Rana et al., 2017). mouse-anti-dsDNA 1;250 (ab27156, abcam); rabbit-anti-PH3 1:1000 (Millipore). Samples were then rinsed 3 times in PBST for 10 min. and incubated with the secondary antibodies and/or stains at room temperature for 3 hours. Secondary antibodies used were: anti-rabbit or anti-mouse AlexaFluor-488 1:500 (Invitrogen); anti-rabbit or anti-mouse AlexaFluor-555 1:500 (Invitrogen); To-Pro-3 DNA stain 1:500 (Invitrogen); 4,6-diamidino-2-phenylindole (DAPI) 1:2000; phalloidin AlexaFlour-568 1:250 (Invitrogen). Finally, samples were rinsed 3 times with PBST for 10 min. and mounted in Vectashield Mounting Medium (Vector Lab). Images were taken using Zeiss LSM780 or LSM880 confocal microscope and analyzed using the ImageJ software to measure intensity, mitochondrial area, and aggregates sizes. The image of mitochondria in guts were taken from the posterior midgut R5 region by Buchon et al.. The number of PH3+ cells were counted in whole midguts, defined from R1 to R5.

TMRE staining

Flies were anesthetized and dissected in cold Drosophila Schneider's Medium (DSM). Brain and hemi-thoraces were incubated in TMRE staining solution (100nm TMRE (T669, Thermo Fisher Scientific) in DSM) for 12 min. at room temperature. After staining samples were rinsed once in wash solution (25nm TMRE in DSM) for 30 s. Hemi-thoraces were mounted in wash solution. Images were acquired in a Zeiss LSM780 confocal using identical setting for each condition. TMRE intensity was quantified using ImageJ software.

GFP-mCherry-Atg8a tandem and Mito-QC staining

Flies were anesthetized and dissected in cold Drosophila Schneider's Medium (DSM). Brains were mounted in DSM solution. Images were acquired in a Zeiss LSM780 or LSM880 confocal using identical setting for each condition. Autolysosomes or mitolysosomes (mCherry-only foci) were quantified using same parameters in the image calculator option in ImageJ software

Intestinal barrier dysfunction (Smurf) assay

Intestinal integrity assay was performed as previously described (Rera et al., 2012). Flies were aged in normal food until the day of the assay. The day before to the assay flies were transferred to new vials containing standard medium with 2.5% wt/vol F&D blue dye # 1 (SPS Alfachem). Flies were kept in this medium for 16 hours and flies with dye coloration outside the gut (Smurf flies) were counted.

Mitochondrial DNA measurement

Total cellular DNA from 10 heads were prepared by homogenization in 10 mM Tris-HCl, pH 8.0, 1 mM EDTA, 0.1% Triton X-100 and 10 □/□ proteinase K. Following 60 min incubation at 37 ℃, Proteinase K was heat inactivated at 95 ℃ for 5 min. Mitochondrial DNA was quantified relative to nuclear DNA by the ratio of amplicons of cytochrome oxidase subunit I (COI) to amplicons of glyceraldehyde 3-phosphate dehydrogenase (GAPDH) in quantitative real-time PCRs. Primer sequences: COI, GAATTAGGACATCCTGGAGC and GCACTAATCAATTTCCAAATCC; GAPDH, GACGAAATCAAGGCTAAGGTCG and AATGGGTGTCGCTGAAGAAGTC.

Climbing activity assay

In negative geotaxis assays, flies were gently tapped to the bottom of 10 cm vials. After 10 seconds, the number of flies that climbed above 5 cm were recorded and compared. For forced climbing assays, 100 adult female flies were placed in 200 ml glass cylinder. Cylinder was tapped quickly and flies were allowed to settle for 2 min. This step was repeated eight times. Then cylinder was tapped quickly and after 1 min, the number of flies in upper, middle, and lower 1/3rd part of the cylinder was recorded.

Spontaneous physical activity assay

10 adult female flies were placed in a Drosophila activity monitor (TriKinetics). Movements were recorded continuously under normal culturing conditions for 36 h on a 12h:12h dark:light cycle. Bar graphs represent mean activity per fly per hour and the scatterplot shows spontaneous activity per fly during 12h:12h dark:light cycle. Triplicate samples were used for each activity measurement

Consumption-Excretion (Con-Ex) assay

Con-EX assay was performed as previously described (Shell et al., 2018). Adult flies were transferred to new empty vial (10 flies per each vial, total 6 vials) and fed from feeder cap containing standard medium with 2.5% wt/vol F&D blue dye # 1 for 20h at 25 ℃. Feeder caps were discarded at the conclusion of feeding. For checking internal dye, the dye inside the flies was collected via homogenization of animal in 500□ of dH2O and pellet debris were removed by centrifugation. The dye excreted by the flies in the walls of the vials was collected by additional 1ml of dH2O to vial followed by vortex.

Fecundity assay

Flies were collected and kept in a humidified, temperature- controlled incubator with 12h:12h dark:light cycle at 25 °C. Eggs laid per fly in 24 h were counted.

Quantitative PCR for 16 S ribosomal RNA

Genomic DNA was extracted using the PowerSoil DNA isolation kit (MoBio). All flies were surface sterilized as previously described prior to sample preparation. To ensure consistent homogenization, 10 flies were pre-homogenized in 150 □ of solution from the PowerSoil bead tube using a motor pestle. Then the homogenate was returned to the bead tube and the manufacturers protocol was followed. PCR was

performed with PowerUP SYBR Green Master Mix (Ref#A25777, Applied Biosystems) on a CFX96Real Time PCR system. Cycling condition were as follows: 95℃ for 15 s then 60℃ for 60 s, cycled 40 times. The 16S gene expression values were normalized to the value of the loading control gene Actin5C. Primer sequences: Act5C, TTGTCTGGGCAAGAGGATCAG and ACCACTCGCACTTGCACTTTC.

Universal primers for the 16 S ribosomal RNA gene were against variable regions 1 (V1F) and 2 (V2R), as previously published (Clark et al., 2015).

Statistics

GraphPad Prism 6 (GraphPad Software, La Jolla, CA, USA) was used to perform the statistical analysis and graphical display of the data. Significance is expressed as *p* values. For comparisons of two groups, an unpaired *t* test was used. Bar graph depicts mean ± standard error of the mean (SEM). The number (n) of biological samples used in each experiment and what n represents can be found in each figure legend. Log-rank test was used for survival curves comparison. Physiological and biochemical results were compared by Student's *t* test or ANOVA with Bonferroni post hoc tests. The difference between two groups was defined as statistically significant for the following *p* values: **p*<0.05, ***p*<0.01, ****p*< 0.001, and non-significant (n.s.) *p*>0.05. No methods were used to determine whether the data met assumptions of the statistical approach.

Declarations

Acknowledgments

We thank Zhuohua Zhang (Xiangya Medical School), Eric Baehrecke (UMass Medical School), Vienna *Drosophila* RNAi Center, and the *Drosophila* Stock Center (Bloomington) for fly stocks; José Armando Guerrero and Vishal Patel for help with fly work. Stocks obtained from the Bloomington *Drosophila* Stock Center (NIH P40OD018537) were used in this study. This work was supported by NIH grants (R01AG037514, R01AG049157) to D.W.W. This research was conducted while D.W.W. was a Julie Martin Mid-Career Awardee in Aging Research supported by The Ellison Medical Foundation and AFAR.

References

Alexander, G.E., Ryan, L., Bowers, D., Foster, T.C., Bizon, J.L., Geldmacher, D.S., and Glisky, E.L. (2012). Characterizing cognitive aging in humans with links to animal models. Front Aging Neurosci *4*, 21.

Aparicio, R., Rana, A., and Walker, D.W. (2019). Upregulation of the Autophagy Adaptor p62/SQSTM1 Prolongs Health and Lifespan in Middle-Aged Drosophila. Cell Rep *28*, 1029-1040 e1025.

Bellot, G., Garcia-Medina, R., Gounon, P., Chiche, J., Roux, D., Pouyssegur, J., and Mazure, N.M. (2009). Hypoxia-induced autophagy is mediated through hypoxia-inducible factor induction of BNIP3 and BNIP3L via their BH3 domains. Mol Cell Biol *29*, 2570-2581.

Biteau, B., Hochmuth, C.E., and Jasper, H. (2008). JNK activity in somatic stem cells causes loss of tissue homeostasis in the aging Drosophila gut. Cell Stem Cell *3*, 442-455.

Brandt, T., Mourier, A., Tain, L.S., Partridge, L., Larsson, N.G., and Kuhlbrandt, W. (2017). Changes of mitochondrial ultrastructure and function during ageing in mice and Drosophila. Elife *6*.

Burton, T.R., and Gibson, S.B. (2009). The role of Bcl-2 family member BNIP3 in cell death and disease: NIPping at the heels of cell death. Cell Death Differ *16*, 515-523.

Chang, J.T., Kumsta, C., Hellman, A.B., Adams, L.M., and Hansen, M. (2017). Spatiotemporal regulation of autophagy during Caenorhabditis elegans aging. Elife *6*.

Cho, J., Hur, J.H., and Walker, D.W. (2011). The role of mitochondria in Drosophila aging. Exp Gerontol *46*, 331-334.

Clark, R.I., Salazar, A., Yamada, R., Fitz-Gibbon, S., Morselli, M., Alcaraz, J., Rana, A., Rera, M., Pellegrini, M., Ja, W.W*., et al.* (2015). Distinct Shifts in Microbiota Composition during Drosophila Aging Impair Intestinal Function and Drive Mortality. Cell Rep *12*, 1656-1667.

D'Amico, D., Mottis, A., Potenza, F., Sorrentino, V., Li, H., Romani, M., Lemos, V., Schoonjans, K., Zamboni, N., Knott, G*., et al.* (2019). The RNA-Binding Protein PUM2 Impairs Mitochondrial Dynamics and Mitophagy During Aging. Mol Cell *73*, 775-787 e710.

Dambroise, E., Monnier, L., Ruisheng, L., Aguilaniu, H., Joly, J.S., Tricoire, H., and Rera, M. (2016). Two phases of aging separated by the Smurf transition as a public path to death. Sci Rep *6*, 23523.

Demontis, F., and Perrimon, N. (2010). FOXO/4E-BP signaling in Drosophila muscles regulates organism-wide proteostasis during aging. Cell *143*, 813-825.

Dorn, G.W., 2nd (2010). Mitochondrial pruning by Nix and BNip3: an essential function for cardiac-expressed death factors. J Cardiovasc Transl Res *3*, 374-383.

Drummond, M.J., Addison, O., Brunker, L., Hopkins, P.N., McClain, D.A., LaStayo, P.C., and Marcus, R.L. (2014). Downregulation of E3 ubiquitin ligases and mitophagy-related genes in skeletal muscle of physically inactive, frail older women: a cross-sectional comparison. J Gerontol A Biol Sci Med Sci *69*, 1040-1048.

Dykiert, D., Der, G., Starr, J.M., and Deary, I.J. (2012). Age differences in intra-individual variability in simple and choice reaction time: systematic review and meta-analysis. PLoS One *7*, e45759.

Feng, Y., He, D., Yao, Z., and Klionsky, D.J. (2014). The machinery of macroautophagy. Cell Res *24*, 24-41.

Ferguson, M., Mockett, R.J., Shen, Y., Orr, W.C., and Sohal, R.S. (2005). Age-associated decline in mitochondrial respiration and electron transport in Drosophila melanogaster. Biochem J *390*, 501-511.

Gao, A., Jiang, J., Xie, F., and Chen, L. (2020). Bnip3 in mitophagy: Novel insights and potential therapeutic target for diseases of secondary mitochondrial dysfunction. Clin Chim Acta *506*, 72-83.

Glick, D., Zhang, W., Beaton, M., Marsboom, G., Gruber, M., Simon, M.C., Hart, J., Dorn, G.W., 2nd, Brady, M.J., and Macleod, K.F. (2012). BNip3 regulates mitochondrial function and lipid metabolism in the liver. Mol Cell Biol *32*, 2570-2584.

Grimm, A., and Eckert, A. (2017). Brain aging and neurodegeneration: from a mitochondrial point of view. J Neurochem *143*, 418-431.

Hanna, R.A., Quinsay, M.N., Orogo, A.M., Giang, K., Rikka, S., and Gustafsson, A.B. (2012). Microtubule-associated protein 1 light chain 3 (LC3) interacts with Bnip3 protein to selectively remove endoplasmic reticulum and mitochondria via autophagy. J Biol Chem *287*, 19094-19104.

Hansen, M., Rubinsztein, D.C., and Walker, D.W. (2018). Autophagy as a promoter of longevity: insights from model organisms. Nat Rev Mol Cell Biol *19*, 579-593.

Hu, D.J., and Jasper, H. (2017). Epithelia: Understanding the Cell Biology of Intestinal Barrier Dysfunction. Curr Biol *27*, R185-R187.

Jasper, H. (2015). Exploring the physiology and pathology of aging in the intestine of Drosophila melanogaster. Invertebr Reprod Dev *59*, 51-58.

Kale, J., Osterlund, E.J., and Andrews, D.W. (2018). BCL-2 family proteins: changing partners in the dance towards death. Cell Death Differ *25*, 65-80.

Kavanagh, K., Brown, R.N., Davis, A.T., Uberseder, B., Floyd, E., Pfisterer, B., and Shively, C.A. (2016). Microbial translocation and skeletal muscle in young and old vervet monkeys. Age (Dordr) *38*, 58.

Klionsky, D.J., Abdel-Aziz, A.K., Abdelfatah, S., Abdellatif, M., Abdoli, A., Abel, S., Abeliovich, H., Abildgaard, M.H., Abudu, Y.P., Acevedo-Arozena, A.*, et al.* (2021). Guidelines for the use and interpretation of assays for monitoring autophagy (4th edition)(1). Autophagy *17*, 1-382.

Kubli, D.A., Ycaza, J.E., and Gustafsson, A.B. (2007). Bnip3 mediates mitochondrial dysfunction and cell death through Bax and Bak. Biochem J *405*, 407-415.

Lee, J.J., Sanchez-Martinez, A., Martinez Zarate, A., Beninca, C., Mayor, U., Clague, M.J., and Whitworth, A.J. (2018). Basal mitophagy is widespread in Drosophila but minimally affected by loss of Pink1 or parkin. J Cell Biol *217*, 1613-1622.

Lee, T.V., Kamber Kaya, H.E., Simin, R., Baehrecke, E.H., and Bergmann, A. (2016). The initiator caspase Dronc is subject of enhanced autophagy upon proteasome impairment in Drosophila. Cell Death Differ *23*, 1555-1564.

Levin, O., Fujiyama, H., Boisgontier, M.P., Swinnen, S.P., and Summers, J.J. (2014). Aging and motor inhibition: a converging perspective provided by brain stimulation and imaging approaches. Neurosci Biobehav Rev *43*, 100-117.

Levine, B., and Kroemer, G. (2008). Autophagy in the pathogenesis of disease. Cell *132*, 27-42.

Li, H., and Jasper, H. (2016). Gastrointestinal stem cells in health and disease: from flies to humans. Dis Model Mech *9*, 487-499.

Li, R., Xin, T., Li, D., Wang, C., Zhu, H., and Zhou, H. (2018). Therapeutic effect of Sirtuin 3 on ameliorating nonalcoholic fatty liver disease: The role of the ERK-CREB pathway and Bnip3-mediated mitophagy. Redox Biol *18*, 229-243.

Lopez-Otin, C., Blasco, M.A., Partridge, L., Serrano, M., and Kroemer, G. (2013). The hallmarks of aging. Cell *153*, 1194-1217.

Lou, G., Palikaras, K., Lautrup, S., Scheibye-Knudsen, M., Tavernarakis, N., and Fang, E.F. (2020). Mitophagy and Neuroprotection. Trends Mol Med *26*, 8-20.

Martinez-Vicente, M. (2017). Neuronal Mitophagy in Neurodegenerative Diseases. Front Mol Neurosci *10*, 64.

Mattson, M.P., and Arumugam, T.V. (2018). Hallmarks of Brain Aging: Adaptive and Pathological Modification by Metabolic States. Cell Metab *27*, 1176-1199.

McWilliams, T.G., Prescott, A.R., Allen, G.F., Tamjar, J., Munson, M.J., Thomson, C., Muqit, M.M., and Ganley, I.G. (2016). mito-QC illuminates mitophagy and mitochondrial architecture in vivo. J Cell Biol *214*, 333-345.

Miller, H.A., Dean, E.S., Pletcher, S.D., and Leiser, S.F. (2020). Cell non-autonomous regulation of health and longevity. Elife *9*.

Nakatogawa, H., Suzuki, K., Kamada, Y., and Ohsumi, Y. (2009). Dynamics and diversity in autophagy mechanisms: lessons from yeast. Nat Rev Mol Cell Biol *10*, 458-467.

O'Sullivan, T.E., Johnson, L.R., Kang, H.H., and Sun, J.C. (2015). BNIP3- and BNIP3L-Mediated Mitophagy Promotes the Generation of Natural Killer Cell Memory. Immunity *43*, 331-342.

Onishi, M., Yamano, K., Sato, M., Matsuda, N., and Okamoto, K. (2021). Molecular mechanisms and physiological functions of mitophagy. EMBO J *40*, e104705.

Osterwalder, T., Yoon, K.S., White, B.H., and Keshishian, H. (2001). A conditional tissue-specific transgene expression system using inducible GAL4. P Natl Acad Sci USA *98*, 12596-12601.

Palikaras, K., Lionaki, E., and Tavernarakis, N. (2015). Coupling mitogenesis and mitophagy for longevity. Autophagy *11*, 1428-1430.

Palikaras, K., Lionaki, E., and Tavernarakis, N. (2016). Mitophagy: In sickness and in health. Mol Cell Oncol *3*, e1056332.

Palikaras, K., Lionaki, E., and Tavernarakis, N. (2018). Mechanisms of mitophagy in cellular homeostasis, physiology and pathology. Nat Cell Biol *20*, 1013-1022.

Partridge, L., Gems, D., and Withers, D.J. (2005). Sex and death: what is the connection? Cell *120*, 461-472.

Pickles, S., Vigie, P., and Youle, R.J. (2018). Mitophagy and Quality Control Mechanisms in Mitochondrial Maintenance. Curr Biol *28*, R170-R185.

Pickrell, A.M., and Youle, R.J. (2015). The Roles of PINK1, Parkin, and Mitochondrial Fidelity in Parkinson's Disease. Neuron *85*, 257-273.

Poirier, L., Shane, A., Zheng, J., and Seroude, L. (2008). Characterization of the Drosophila gene-switch system in aging studies: a cautionary tale. Aging Cell *7*, 758-770.

Prince, M.J., Wu, F., Guo, Y., Gutierrez Robledo, L.M., O'Donnell, M., Sullivan, R., and Yusuf, S. (2015). The burden of disease in older people and implications for health policy and practice. Lancet *385*, 549-562.

Rana, A., Oliveira, M.P., Khamoui, A.V., Aparicio, R., Rera, M., Rossiter, H.B., and Walker, D.W. (2017). Promoting Drp1-mediated mitochondrial fission in midlife prolongs healthy lifespan of Drosophila melanogaster. Nat Commun *8*, 448.

Rana, A., Rera, M., and Walker, D.W. (2013). Parkin overexpression during aging reduces proteotoxicity, alters mitochondrial dynamics, and extends lifespan. Proc Natl Acad Sci U S A *110*, 8638-8643.

Regula, K.M., Ens, K., and Kirshenbaum, L.A. (2002). Inducible expression of BNIP3 provokes mitochondrial defects and hypoxia-mediated cell death of ventricular myocytes. Circ Res *91*, 226-231.

Rera, M., Azizi, M.J., and Walker, D.W. (2013). Organ-specific mediation of lifespan extension: more than a gut feeling? Ageing Res Rev *12*, 436-444.

Rera, M., Bahadorani, S., Cho, J., Koehler, C.L., Ulgherait, M., Hur, J.H., Ansari, W.S., Lo, T., Jr., Jones, D.L., and Walker, D.W. (2011). Modulation of longevity and tissue homeostasis by the Drosophila PGC-1 homolog. Cell Metab *14*, 623-634.

Rera, M., Clark, R.I., and Walker, D.W. (2012). Intestinal barrier dysfunction links metabolic and inflammatory markers of aging to death in Drosophila. Proc Natl Acad Sci U S A *109*, 21528-21533.

Rikka, S., Quinsay, M.N., Thomas, R.L., Kubli, D.A., Zhang, X., Murphy, A.N., and Gustafsson, A.B. (2011). Bnip3 impairs mitochondrial bioenergetics and stimulates mitochondrial turnover. Cell Death Differ *18*, 721-731.

Ryu, D., Mouchiroud, L., Andreux, P.A., Katsyuba, E., Moullan, N., Nicolet-Dit-Felix, A.A., Williams, E.G., Jha, P., Lo Sasso, G., Huzard, D.*, et al.* (2016). Urolithin A induces mitophagy and prolongs lifespan in C. elegans and increases muscle function in rodents. Nat Med *22*, 879-888.

Schinaman, J.M., Rana, A., Ja, W.W., Clark, R.I., and Walker, D.W. (2019). Rapamycin modulates tissue aging and lifespan independently of the gut microbiota in Drosophila. Sci Rep *9*, 7824.

Shell, B.C., Schmitt, R.E., Lee, K.M., Johnson, J.C., Chung, B.Y., Pletcher, S.D., and Grotewiel, M. (2018). Measurement of solid food intake in Drosophila via consumption-excretion of a dye tracer. Sci Rep *8*, 11536.

Sun, N., Youle, R.J., and Finkel, T. (2016). The Mitochondrial Basis of Aging. Mol Cell *61*, 654-666.

Sun, N., Yun, J., Liu, J., Malide, D., Liu, C., Rovira, II, Holmstrom, K.M., Fergusson, M.M., Yoo, Y.H., Combs, C.A.*, et al.* (2015). Measuring In Vivo Mitophagy. Mol Cell *60*, 685-696.

Tang, C., Han, H., Liu, Z., Liu, Y., Yin, L., Cai, J., He, L., Liu, Y., Chen, G., Zhang, Z.*, et al.* (2019). Activation of BNIP3-mediated mitophagy protects against renal ischemia-reperfusion injury. Cell Death Dis *10*, 677.

Thevaranjan, N., Puchta, A., Schulz, C., Naidoo, A., Szamosi, J.C., Verschoor, C.P., Loukov, D., Schenck, L.P., Jury, J., Foley, K.P.*, et al.* (2017). Age-Associated Microbial Dysbiosis Promotes Intestinal Permeability, Systemic Inflammation, and Macrophage Dysfunction. Cell Host Microbe *21*, 455-466 e454.

Ulgherait, M., Rana, A., Rera, M., Graniel, J., and Walker, D.W. (2014). AMPK Modulates Tissue and Organismal Aging in a Non-Cell-Autonomous Manner. Cell Rep *8*, 1767-1780.

Walker, D.W., and Benzer, S. (2004). Mitochondrial "swirls" induced by oxygen stress and in the Drosophila mutant hyperswirl. Proc Natl Acad Sci U S A *101*, 10290-10295.

Weir, H.J., and Mair, W.B. (2016). SnapShot: Neuronal Regulation of Aging. Cell *166*, 784-784 e781.

Youle, R.J., and Narendra, D.P. (2011). Mechanisms of mitophagy. Nat Rev Mol Cell Biol *12*, 9-14.

Zhang, J., and Ney, P.A. (2009). Role of BNIP3 and NIX in cell death, autophagy, and mitophagy. Cell Death Differ *16*, 939-946.

Zhang, T., Xue, L., Li, L., Tang, C., Wan, Z., Wang, R., Tan, J., Tan, Y., Han, H., Tian, R.*, et al.* (2016). BNIP3 Protein Suppresses PINK1 Kinase Proteolytic Cleavage to Promote Mitophagy. J Biol Chem *291*, 21616-21629.

Zhu, Y., Massen, S., Terenzio, M., Lang, V., Chen-Lindner, S., Eils, R., Novak, I., Dikic, I., Hamacher-Brady, A., and Brady, N.R. (2013). Modulation of serines 17 and 24 in the LC3-interacting region of Bnip3 determines pro-survival mitophagy versus apoptosis. J Biol Chem *288*, 1099-1113.

Figures

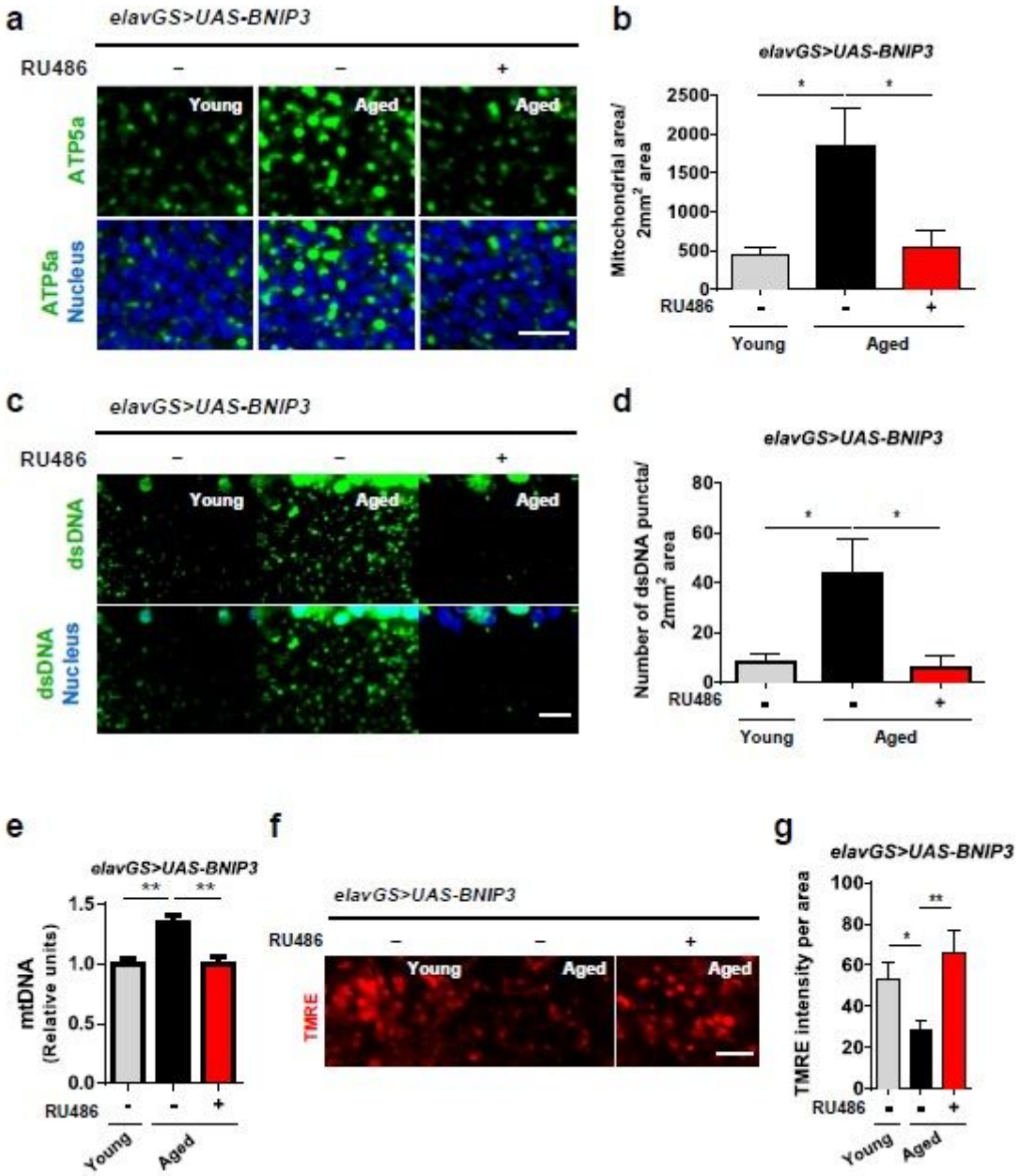

Figure 1

Neuronal BNIP3 induction prevents accumulation of dysfunctional mitochondria in the aged brain. (a) Immunostaining of brains from young (10-day-old) and aged (30-day-old) elavGS>UAS-BNIP3 flies with or without RU486-mediated transgene induction from day 5 onward, showing mitochondrial morphology (green channel, anti-ATP5a) and nuclear DNA (blue channel, stained with To-Pro-3). Scale bar is 5 μ. (b)

Quantification of mitochondrial area in brain as shown in (a). n = 5-9 flies. *p<0.05; unpaired t test. (c) Immunostaining of brains from young (10-day-old) and aged (30-day-old) elavGS>UAS-BNIP3 flies with or without RU486-mediated transgene induction from day 5 onward, showing mitochondrial DNA (green channel, anti-dsDNA) and nuclear DNA (blue channel, stained with To-Pro-3). Scale bar is 5 □. (d) Quantification of mitochondrial DNA in brain as shown in (c). n = 6-7 flies. *p<0.05; unpaired t test. (e) Mitochondrial DNA (mtDNA) amount in brains of young (10-day-old) and aged (30-day-old) elavGS>UAS-BNIP3 flies as determined by quantitative PCR. *p<0.05; unpaired t test. Units are relative to the amounts of a nuclear DNA (nDNA) amplicon (n = 10, per replicate). (f) Staining of brains from young (10-day-old) and aged (30-day-old) elavGS>UAS-BNIP3 flies with or without RU486-mediated transgene induction from day 5 onward, showing TMRE fluorescence. Scale bar is 5 □. (g) Quantification of mitochondrial membrane potential measured by TMRE staining as shown in (f). n = 6-8 flies. *p<0.05, **p<0.01; unpaired t test. RU486 was provided in the media at a concentration of 5 □/□. Error bars represent SEM

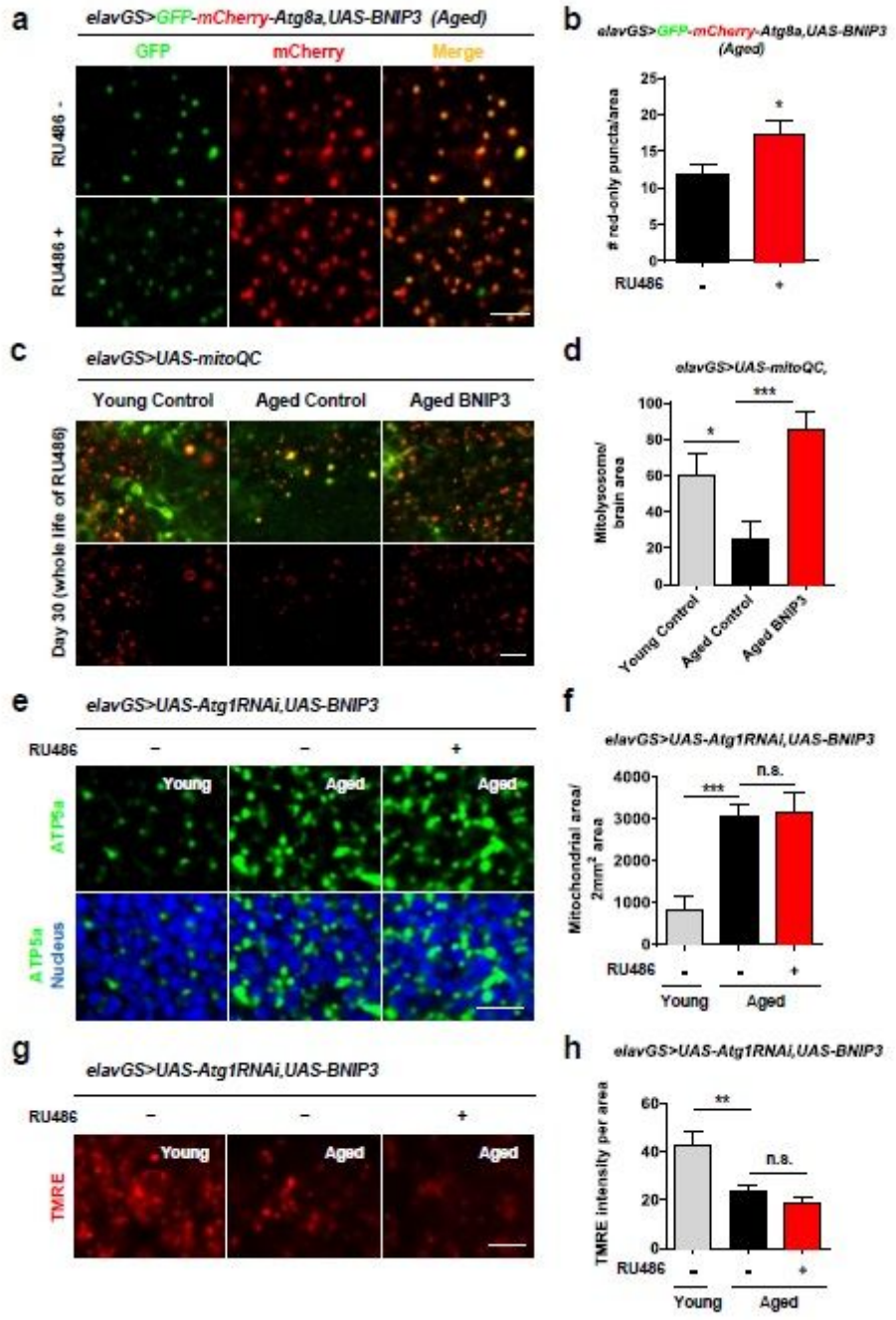

Figure 2

Neuronal BNIP3 induction induces mitophagy to improve mitochondrial homeostasis. (a) GFP-mCherry-ATG8a of brains from 51-day-old elavGS>GFP-mCherry-ATG8a,UAS-BNIP3 flies. Images shown of GFP, mCherry, and merged GFP-mCherry channels. (b) Quantification of autolysosomes (red-only puncta) in brains as shown in (a). n = 7-8 flies. *p<0.05; unpaired t test (c) mito-QC of brains from 30-day-old flies. Genotypes analyzed were elavGS>UAS-mito-QC,UAS-lacZ, as a control, and elavGS>UAS-mito-QC,UAS-BNIP3 flies with RU486-mediated transgene induction from day 5 onwards. Images shown of merged GFP and mCherry along with punctate mCherry-only foci (from merged images where GFP has been quenched; mitolysosomes). Scale bar is 5 □. (d) Quantification of mitolysosomes in brains as shown in (c). n > 10 flies. *p<0.05; **p<0.01; unpaired t test. (e) Immunostaining of brains from young (10-day-old)

and aged (30-day-old) elavGS>UAS-Atg1RNAi,UAS-BNIP3 flies with or without RU486-mediated transgene induction from day 5 onward, showing mitochondrial morphology (green channel, anti-ATP5a) and nuclear DNA (blue channel, stained with To-Pro-3). Scale bar is 5□. (f) Quantification of mitochondrial area in brain as shown in (e). n = 6-9 flies. ***p<0.001, non-significant (n.s.); unpaired t test. (g) Staining of brains from young (10-day-old) and aged (51-day-old) elavGS>UAS-Atg1RNAi,UAS-BNIP3 flies with or without RU486-mediated transgene induction from day 5 onward, showing TMRE fluorescence. Scale bar is 5 □. (h) Quantification of mitochondrial membrane potential measured by TMRE staining as shown in (g). n = 4-7 flies. *p<0.05, non-significant (n.s.); unpaired t test. RU486 was provided in the media at a concentration of 5 □/□. Error bars represent SEM.

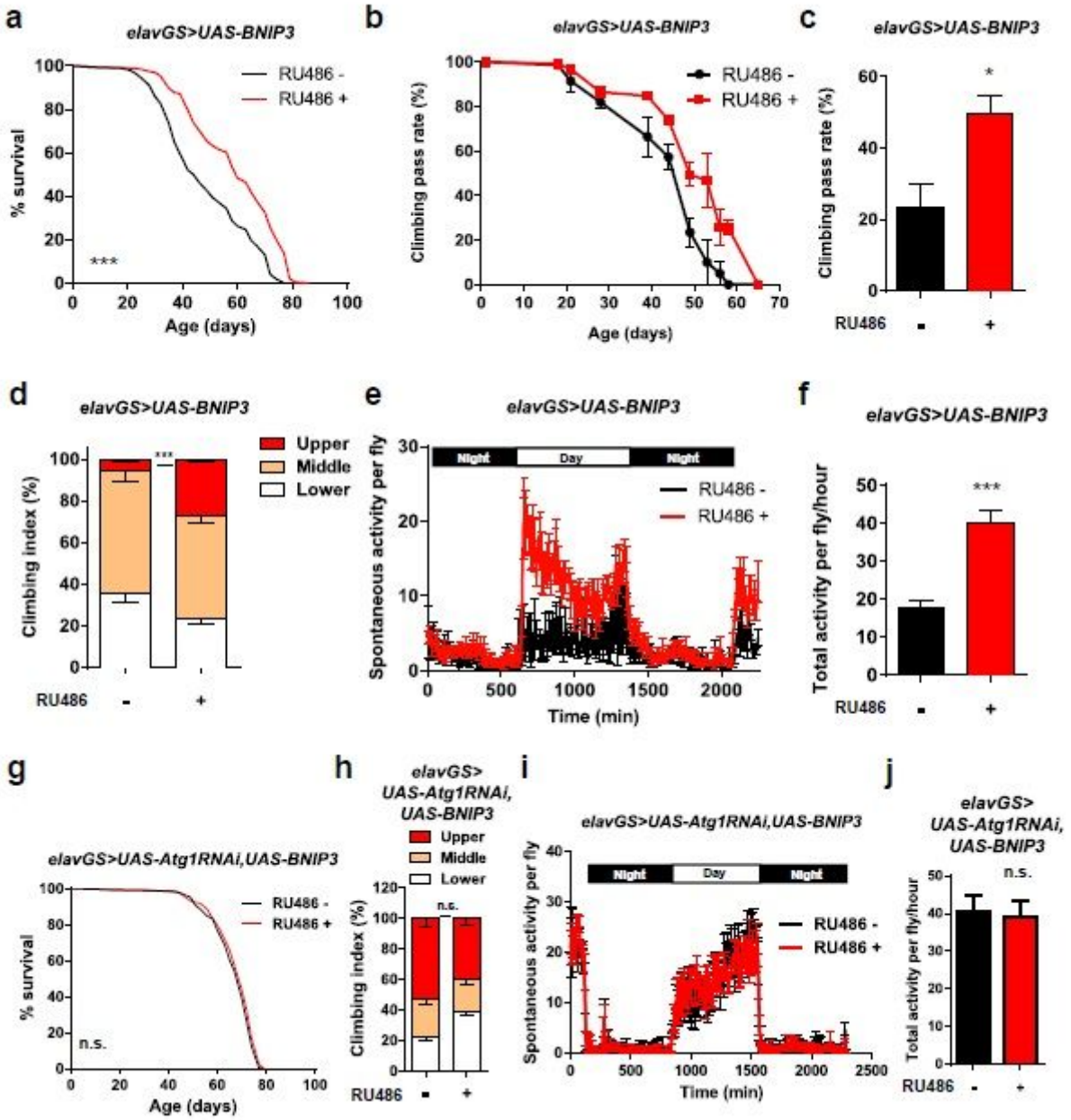

Figure 3

Neuronal BNIP3 induction extends lifespan and improves healthspan. (a) Survival curves of elavGS>UAS-BNIP3 flies with or without RU486-mediated transgene induction from day 5 onward. ***p<0.001; log-rank test; n > 146 flies. (b) Climbing pass rate of elavGS>UAS-BNIP3 flies during aging with or without RU486-mediated transgene induction from day 5 onward; n > 145 flies. (c) Climbing pass rate of 49-day-old elavGS>UAS-BNIP3 flies with or without RU486-mediated transgene induction from day 5 onward. *p<0.05; unpaired t test. (d) Climbing index as a measure of endurance of 37-day-old elavGS>UAS-BNIP3 flies with or without RU486-mediated transgene induction from day 5 onward. n > 4 biological replicates with 100 flies per replicate. ***p < 0.001; unpaired t test. (e) Spontaneous physical activity of 37-day-old elavGS>UAS-BNIP3 flies with or without RU486-mediated transgene induction from day 5 onward. n = 3 vials of 10 flies per condition (f) Quantification of total activity per fly per hour from spontaneous activity graphs (e). n = 3 vials of 10 flies per condition. ***p<0.001; unpaired t test. (g) Survival curves of elavGS>UAS-Atg1RNAi,UAS-BNIP3 flies with or without RU486-mediated transgene induction from day 5 onward. non-significant (n.s.); log-rank test. n > 222 flies. (h) Climbing index as a measure of endurance of 51-day-old elavGS>UAS-Atg1RNAi,UAS-BNIP3 flies with or without RU486-mediated transgene induction from day 5 onward. n = 8 biological replicates with 100 flies per replicate. non-significant (n.s.); unpaired t test. (i) Spontaneous physical activity of 51-day-old elavGS>UAS-Atg1RNAi;UAS-BNIP3 flies with or without RU486-mediated transgene induction from day 5 onward. n = 3 vials of 10 flies per condition (j) Quantification of total activity per fly per hour from spontaneous activity graphs (i). n = 3 vials of 10 flies per condition. non-significant (n.s.); unpaired t test. RU486 was provided in the media at a concentration of 5 □/□. Error bars represent SEM.

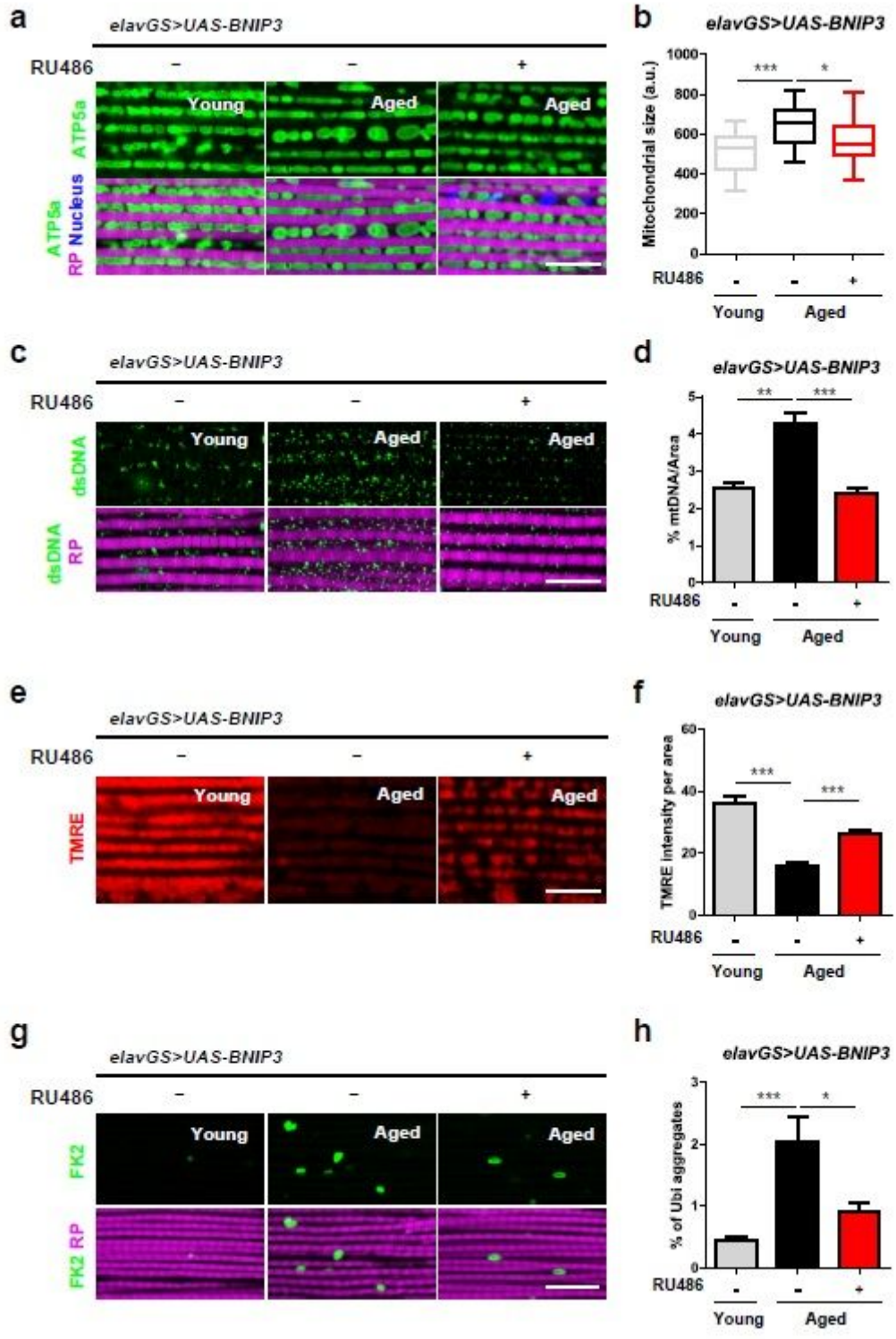

Figure 4

Neuronal BNIP3 induction improves mitochondrial homeostasis and proteostasis in aged muscle. (a) Immunostaining of indirect flight muscles from young (10-day-old) and aged (30-day-old) elavGS>UAS-BNIP3 flies with or without RU486-mediated transgene induction from day 5 onward, showing mitochondrial morphology (green channel, anti-ATP5a) and nuclear DNA (blue channel, stained with DAPI). Scale bar is 10 □. (b) Quantification of mitochondrial area in muscle as shown in (a). n = 8 flies.

*p<0.05, ***p<0.001; unpaired t test. (c) Immunostaining of indirect flight muscles from young (10-day-old) and aged (30-day-old) elavGS>UAS-BNIP3 flies with or without RU486-mediated transgene induction from day 5 onward, showing mitochondrial DNA (green channel, anti-dsDNA) and nuclear DNA (blue channel, stained with DAPI). Scale bar is 10 □. (d) Quantification of mitochondrial DNA in muscle as shown in (c). n =11 flies. **p<0.01, ***p<0.001; unpaired t test. (e) Staining of brains from young (10-day-old) and aged (30-day-old) elavGS>UAS-BNIP3 flies with or without RU486-mediated transgene induction from day 5 onward, showing TMRE fluorescence. Scale bar is 10 □. (f) Quantification of mitochondrial membrane potential measured by TMRE staining as shown in (e). n > 10 flies. ***p<0.001; unpaired t test. (g) Immunostaining of indirect flight muscles from young (10-day-old) and aged (30-day-old) elavGS>UAS-BNIP3 flies with or without RU486-mediated transgene induction from day 5 onward, showing polyubiquitinated aggregates (green channel, anti-FK2) and muscles (magenta channel, stained with phalloidin/F-actin). Scale bar is 10 □. (h) Quantification of polyubiquitin aggregates in muscle as shown in (g). n > 8 flies. *p<0.05, ***p<0.001; unpaired t test. RU486 was provided in the media at a concentration of 5 □/□. Error bars represent Min to Max (b) or SEM (d, f, and h).

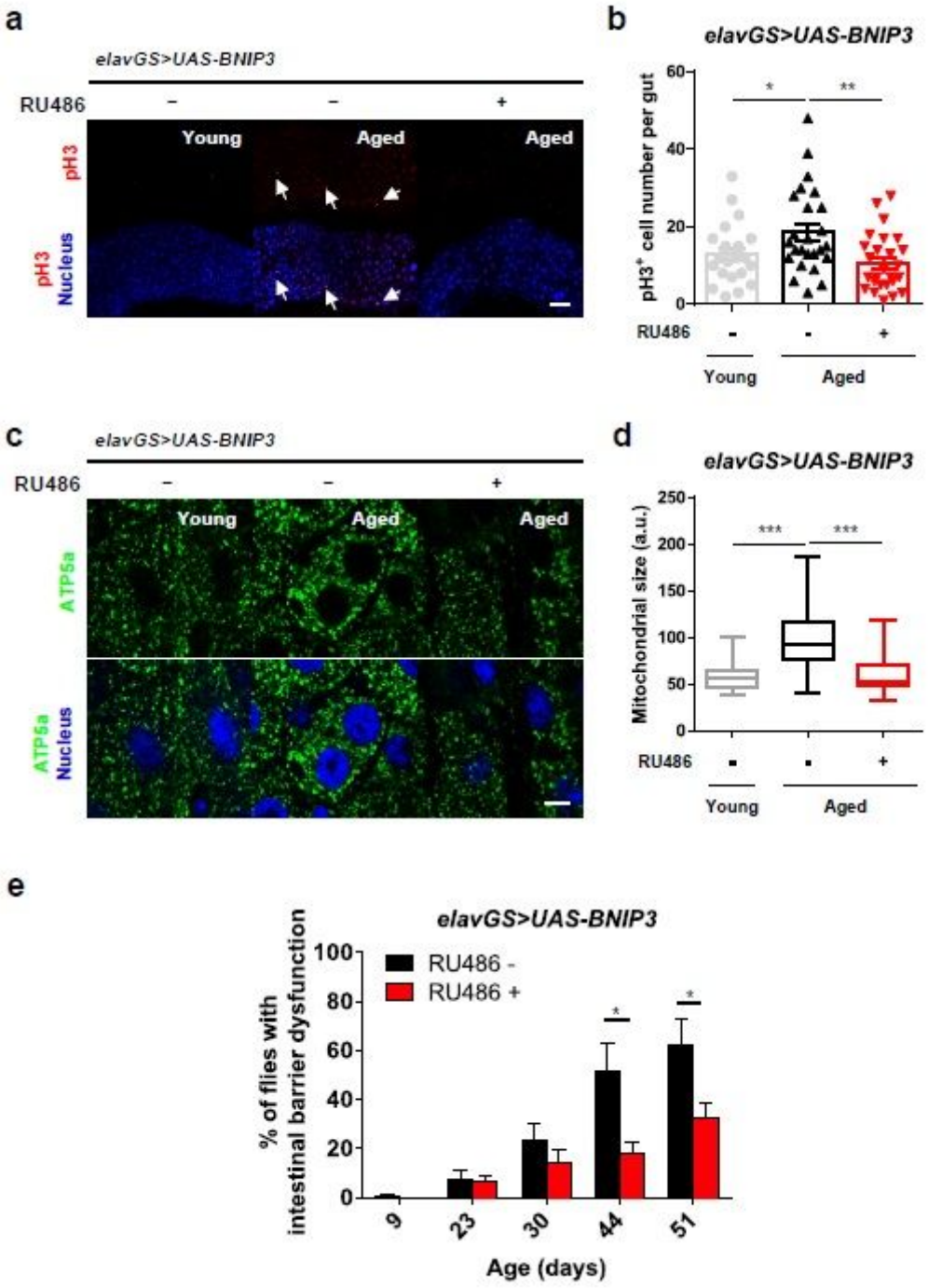

Figure 5

Neuronal BNIP3 induction improves intestinal homeostasis during aging. (a) Immunostaining of guts from young (10-day-old) and aged (30-day-old) elavGS>UAS-BNIP3 flies with or without RU486-mediated transgene induction from day 5 onward, showing intestinal stem cell proliferation (red channel, anti-PH3, white arrows) and nuclear DNA (blue channel, stained with DAPI). Scale bar is 50 □. (b) Quantification of total number of PH3+ cells in gut as shown in (a). n > 23 flies. *p<0.05, **p<0.01; unpaired t test. (c) Immunostaining of guts from young (10-day-old) and aged (30-day-old) elavGS>UAS-BNIP3 flies with or without RU486-mediated transgene induction from day 5 onward, showing mitochondrial morphology

(green channel, anti-ATP5a) and nuclear DNA (blue channel, stained with DAPI). Scale bar is 5 □. (d) Quantification of mitochondrial area in gut as shown in (c). n = 8 flies. ***p<0.001; unpaired t test. (e) Intestinal integrity during aging of elavGS>UAS-BNIP3 flies with or without RU486-mediated transgene induction from day 5 onward. n = 5 vials, 30 flies per vial on day 10. *p<0.05. RU486 was provided in the media at a concentration of 5 □/□. Error bars represent SEM (b, e, and f) or Min to Max (d).

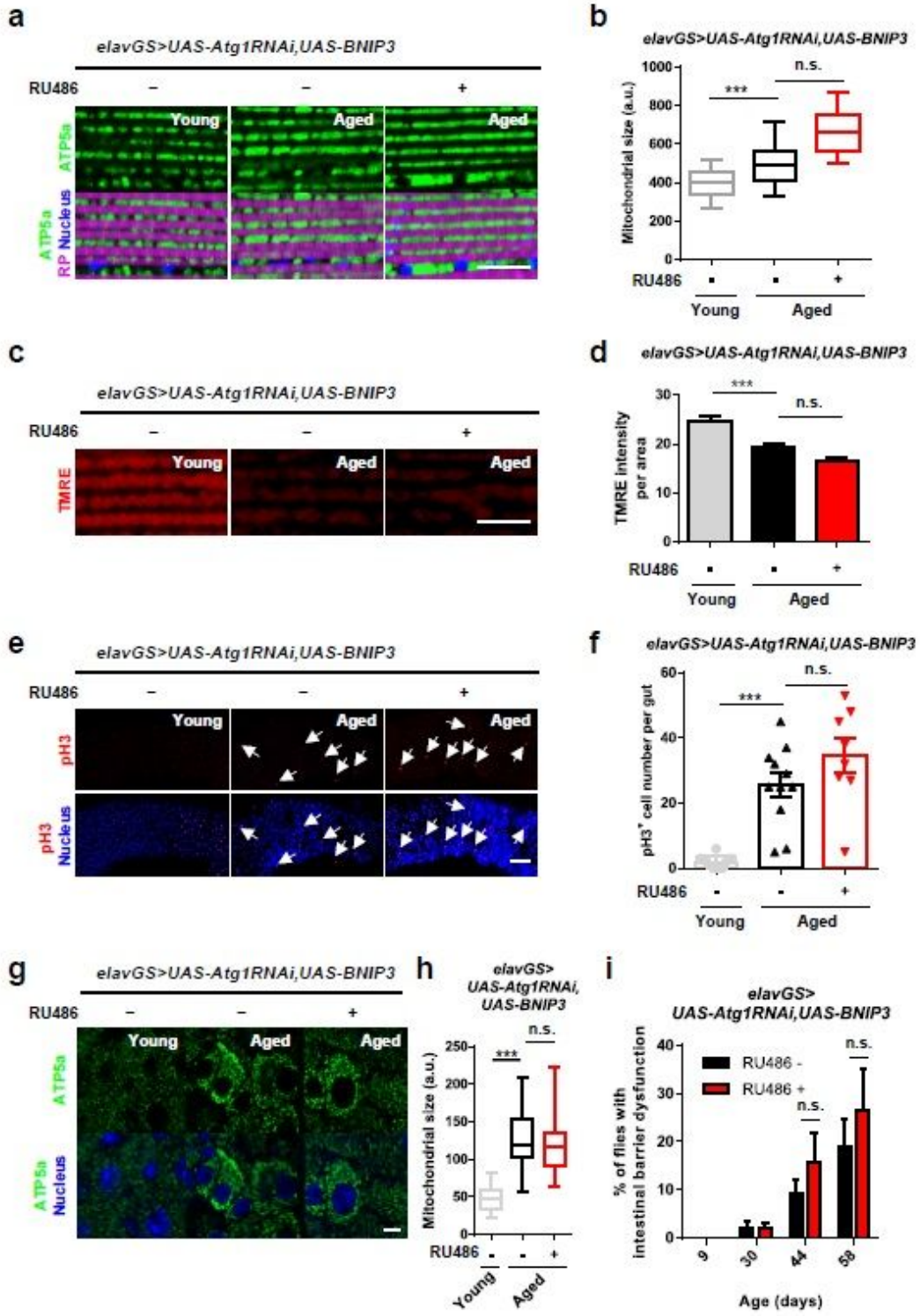

Figure 6

Neuronal BNIP3 induction requires autophagy to delay systemic aging. (a) Immunostaining of indirect flight muscles from young (10-day-old) and aged (30-day-old) elavGS>UAS-Atg1RNAi,UAS-BNIP3 flies with or without RU486-mediated transgene induction from day 5 onward, showing mitochondrial morphology (green channel, anti-ATP5a) and nuclear DNA (blue channel, stained with DAPI). Scale bar is 10 □. (b) Quantification of mitochondrial area in muscle as shown in (a). n = 8 flies. ***p<0.001, non-significant (n.s.); unpaired t test. (c) Staining of indirect flight muscles from young (10-day-old) and aged (51-day-old) elavGS>UAS-BNIP3 flies with or without RU486-mediated transgene induction from day 5 onward, showing TMRE fluorescence. Scale bar is 10 □. (d) Quantification of mitochondrial membrane potential measured by TMRE staining as shown in (c). n > 10 flies. ***p<0.001, non-significant (n.s.); unpaired t test. (e) Immunostaining of guts from young (10-day-old) and aged (51-day-old) elavGS>UAS-Atg1RNAi,UAS-BNIP3 flies with or without RU486-mediated transgene induction from day 5 onward, showing intestinal stem cell proliferation (red channel, anti-PH3, white arrows) and nuclear DNA (blue channel, stained with DAPI). Scale bar is 50 □. (f) Quantification of total number of PH3+ cells in gut as shown in (e). n > 8 flies. ***p<0.001, non-significant (n.s.); unpaired t test. (g) Immunostaining of guts from young (10-day-old) and aged (51-day-old) elavGS>UAS-Atg1RNAi,UAS-BNIP3 flies with or without RU486-mediated transgene induction from day 5 onward, showing mitochondrial morphology (green channel, anti-ATP5a) and nuclear DNA (blue channel, stained with DAPI). Scale bar is 5 □. (h) Quantification of mitochondrial area in gut as shown in (g). n = 8 flies. ***p<0.001, non-significant (n.s.); unpaired t test. (i) Intestinal integrity during aging of elavGS>UAS-Atg1RNAi,UAS-BNIP3 flies with or without RU486-mediated transgene induction from day 5 onward. n = 5 vials, 30 flies per vial on day 10. n.s. = non-significant RU486 was provided in the media at a concentration of 5 □/□. Error bars represent Min to Max (b and h) or SEM (d, f, and i).

Supplementary Files

This is a list of supplementary files associated with this preprint. Click to download.

- ExtendedDataFigurelegends.docx
- ExtendedData.pdf